

$H\alpha + [NII]$ Observations of the HII Regions in M81

Weipeng Lin^{1,2,3}, Xu Zhou^{2,3}, David Burstein⁴, Rogier A. Windhorst⁴, Jiansheng Chen^{2,3},
Wen-ping Chen⁵, Zhaoji Jiang², Xu Kong⁶, Jun Ma², Wei-hsin Sun⁵, Hong Wu², Suijian Xue²,
Jin Zhu²

linwp@center.shao.ac.cn

ABSTRACT

In a first of a series of studies of the $H\alpha + [NII]$ emission from nearby spiral galaxies, we present measurements of $H\alpha + [NII]$ emission from HII regions in M81. Our method uses large-field-CCD images and long-slit spectra, and is part of the ongoing Beijing-Arizona-Taipei-Connecticut Sky Survey (the BATC survey). The CCD images are taken with the NAOC 0.6/0.9m f/3 Schmidt telescope at the Xinglong Observing Station, using a multicolor filter set. Spectra of 10 of the brightest HII regions are obtained using the NAOC 2.16m telescope with a Tek 1024 \times 1024 CCD. The continua of the spectra are calibrated by flux-calibrated images taken from the Schmidt observations. We determine the continuum component of our $H\alpha + [NII]$ image via interpolation from the more accurately-measured backgrounds (M81 starlight) obtained from the two neighboring (in wavelength) BATC filter images. We use the calibrated fluxes of $H\alpha + [NII]$ emission from the spectra to normalize this interpolated, continuum-subtracted $H\alpha + [NII]$ image. We estimate the zero point uncertainty of the measured $H\alpha + [NII]$ emission flux to be $\sim 8\%$. A catalogue of $H\alpha + [NII]$ fluxes for 456 HII regions is provided, with those fluxes are on a more consistent linear scale than previously available. The logarithmically-binned $H\alpha + [NII]$ luminosity function of HII regions is found to have slope $\alpha = -0.70$, consistent with previous results (which allowed $\alpha = -0.5 \sim -0.8$). From the overall $H\alpha + [NII]$ luminosity of the HII regions, the star formation rate of M81 is found to be $\sim 0.68M_{\odot} \text{ yr}^{-1}$, modulo uncertainty with extinction corrections.

Subject headings: galaxies: individual (M81) –galaxies: photometry – galaxies: emission lines – HII regions

¹The Partner Group of MPI für Astrophysik, Shanghai Astronomical Observatory, Shanghai 200030, China

²National Astronomical Observatories of China, Chinese Academy of Sciences, Beijing 100012, China

³Beijing Astrophysics Center & Department of Astronomy, Peking Univ., Beijing 100871, China

⁴Department of Physics and Astronomy, Box 871504, Arizona State University, Tempe, AZ 85287–1504

⁵Institute of Astronomy, National Central University, Chung-Li, Taiwan

⁶Center for Astrophysics, University of Science and Technology of China, Hefei 230026, China

1. Introduction

Part of the Beijing-Arizona-Taipei-Connecticut (BATC) Sky Survey is to do emission line studies of $H\alpha + [NII]$ emission from large-appearing, nearby spiral galaxies which are well-suited to our imaging setup. M81 is a well-known, nearby Sab galaxy (3.6 Mpc; cf. Freedman et al. 1994) that exhibits both LINER and Seyfert 1 characteristics. It is useful as the first galaxy to study in our program, as many studies have been made of the structure and star-forming regions of M81, as well as of its nucleus (e.g., Keel 1989; Hill et al. 1992; Adler & Westpfahl 1996; Davidge & Courteau 1999; Grossan et al. 2001). The HII regions of M81 have been studied by Hodge & Kennicutt (1983), Stauffer & Bothun (1984), Kaufman et al. (1986, 1987), Garnett & Shields (1987), Petit et al. (1988), and Devereux et al. (1995). However, the existing optical photometry of the HII regions is photographic (Kaufman et al. 1986; Petit et al. 1988, hereafter PKS), which is not sufficiently accurate for $H\alpha + [NII]$ flux determinations.

Devereux, Jacoby, & Ciardullo (1995) previously obtained an $H\alpha + [NII]$ image of M81 using CCD data, in which they point out that a small uncertainty (3%) in the continuum level translates into a large ($\sim 30\%$) uncertainty in the measured $H\alpha + [NII]$ flux. Greenawalt et al. (1998) studied the diffuse ionized gas (DIG) in M81 and attributed about half of the $H\alpha$ (i.e., no $[NII]$) emission to the DIG. In the present paper we combine accurate photometric observations of M81 with new spectroscopic observations of the HII regions to obtain new, independent, measurements of the $H\alpha + [NII]$ flux emitted from M81 HII regions. Section 2 describes the observations and data reduction procedures used for both the images and the spectra, which employ a new method to reduce the uncertainty in the continuum background of our image. This new method results in more accurate measurements of the $H\alpha + [NII]$ flux from the M81 HII regions. We discuss our errors of measurement and some statistical applications our data can provide in Section 3. We summarize our results in Section 4.

2. Observations and Data Reduction

2.1. Spectroscopic observations

Spectra of the nucleus of M81 and its HII regions were obtained using the 2.16m telescope at Xinglong Station of the National Astronomical Observatories of China (NAOC) between 1997 April 9-11. A Zeiss universal spectrograph using a Tek 1024×1024 CCD and a grating of $200\text{\AA}/\text{mm}$ dispersion was used to obtain a spectral resolution of 10.0\AA over the range 4500\AA to 9500\AA , centered near 7000\AA . It was necessary to restrict our spectroscopic observations to the brightest HII regions, owing to the bright background of M81. In most cases, a slit width of $3''$ was chosen to match the seeing disk at Xinglong (typically $\sim 2''$). Often the $4'$ -long slit was rotated to include more than one HII region at one time. As our slit was never free of galaxy light, separate sky exposures were periodically taken.

The data were reduced using the MIDAS package. The response of the instrument was calibrated by standard stars HZ44, HD74721, Feige 98 and Feige 56. The details of the observation and data reduction are described by Kong et al. (1999) and Kong et al. (2000). Table 2.1 gives the 10 HII regions observed spectroscopically. Table 3 gives the results for measurement of $H\alpha + [NII]$ emission from these 10 HII regions derived from these spectra, together with estimated errors.

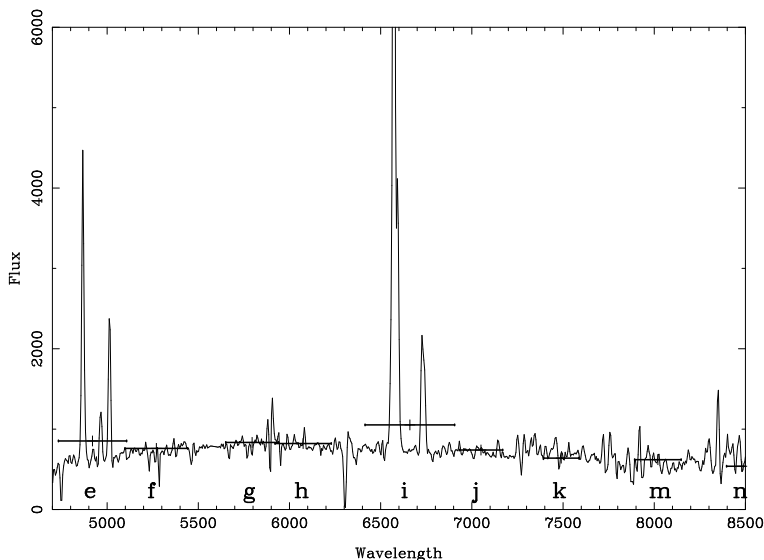


Fig. 1.— An example of spectrum for the M81 HII #16 region listed in Tables 1 and 3. Note that the fluxes in BATC passbands are also shown as thick horizontal lines from left to right for BATC filters e, f, g, h, i, j, k, and m (cf. Zhou et al. 2001; 2003) as well as the narrow $H\alpha$ filter “t”. Calibration of the continuum spectrum was made using the calibrated observations of M81 made in these BATC filters.

2.2. Image observations

The images used in this paper were taken with 0.6/0.9m f/3 Schmidt Telescope of at the Xinglong Observing Station of the National Astronomical Observatories of China (NAOC), equipped with a Ford 2048 \times 2048 CCD camera mounted at its focus. The field of view of the CCD is close to $58' \times 58'$, with a scale of $1.7''/\text{pixel}$. The four filters used for this study are a subset of the 15 intermediate-band filters used for the Beijing-Arizona-Taiwan-Connecticut Multicolor Sky Survey (BATC; cf. Fan et al. 1996, Yan et al. 2000). This filter system was designed to minimize the effect of night sky emission lines, especially those in the near-infrared that are both bright and highly variable. The observations reported here were taken on 30 individual nights over the time period 1995 Feb 5 to 1997 Feb 19. Images in each filter were dithered to provide accurate cosmic ray and defect subtraction. Both M81 and M82 comfortably fit within this field of view.

The $H\alpha$ images were taken by using our “t-filter” (see Table 2), which has a central wavelength

Table 1: Spectral observations of the M81 HII regions

Name of spectrum	PKS # ^a	J2000	Slit width	# Exposures
M81-266	266	09h55m41.1s 68°59'44.7"	3"	1200s × 3
M81-311	311	09h55m53.2s 68°59'04.2"	3"	1200s × 3
M81-178	178	09h55m16.7s 69°08'56.6"	3"	1200s × 3
M81-209	209	09h55m25.0s 69°08'16.4"	3"	1200s × 3
M81-15	15	09h54m39.3s 69°05'26.9"	3"	1200s × 3
M81-16	16,12,19	09h54m39.6s 69°04'47.8"	3"	1200s × 3
M81-17	17	09h54m39.8s 69°05'02.2"	3"	1200s × 3
M81-23	23,25	09h54m41.4s 69°04'07.5"	3"	1200s × 3
M81-29	29,30,31	09h54m42.6s 69°03'36.9"	3"	1200s × 3

^aPKS # refers to the HII region index in the catalog of Petit et al. (1988) paper.

of 6600Å and a full width half-maxima [FWHM] of 120Å. The transmission profile of our t-filter is presented in Fig. 2. As is evident, the t-filter flux includes emission by [NII] line at 6584 Å as well as emission from H α , which is common in such investigations (cf. Devereux et al. 1995). Three of the nominal BATC filters cover this spectral range: the h-filter and j-filter on either side of H α (central wavelengths of 6075Å and 7050Å and FWHM of 310Å and 300Å, respectively), and the i-filter which is a wider filter (FWHM = 480Å) also centered near H α (central wavelength of 6660Å) (the transmission profiles for these filters can be found in Zhou et al. 2003). A total of 51 images were obtained in the 4 filters with a total exposure time of close to 14 hours. The field observed is centered at RA = 09h 55m 35.25s and DEC = 69°21'50.9"(J2000).

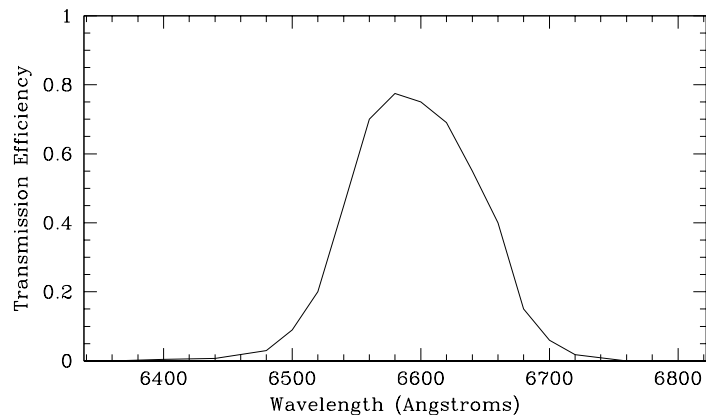


Fig. 2.— The transmission profile of the H α -redshifted t-filter.

Details of the flat-fielding and flux calibration of the BATC CCD system that we employ at

the Xinglong Schmidt telescope have been described in detail elsewhere (cf. Fan et al. 1996; Zheng et al. 1999; Yan et al. 2000; Zhou et al. 2001; Wu et al. 2002; Zhou et al. 2003). The reader is referred to those papers for a detailed description. Calibration of the BATC observations in terms of flux using Oke-Gunn (1983) standard stars is also detailed in Yan et al. (2000). Briefly, our system employs a diffuser plate placed in front of the Schmidt corrector plate to provide a sky-consistent, high-S/N flat field for this CCD system, as sky itself is not flat over the one-degree size scale of our CCD. On nights that are photometric, we observe the Oke-Gunn (1983) primary flux standard stars HD19445, HD84937, BD+262606 and BD+174708 (cf. Yan et al. 2000), which provide us direct calibration of our filter observations in terms of flux.

Table 2: Image observations in H α and nearby bands

Filter	Wavelength(\AA)	FWHM(\AA)	Exposure (s)	# Images	# Calibration Images
t	6600	120	23700	16	...
h	6075	310	8040	10	3
i	6660	480	9960	14	5
j	7050	300	8340	11	4

2.3. Image data reduction

The initial reduction of the images is done by the PIPELINE 1 system software that was developed for automatic data reduction of images taken for the BATC multicolor sky survey (cf. Fan et al. 1996 for details). In the PIPELINE 1 system, images are bias-subtracted, dark-count-subtracted and flat-fielded using multiple biases, dark frames and dome flats taken through the diffusing plate in front of the Schmidt telescope corrector lens. The high accuracy of this procedure has been demonstrated in our previous papers (Fan et al. 1996; Zheng et al. 1999; Yan et al. 2000; Wu et al. 2002). The dithered, flat-fielded images in each passband are combined by integer pixel shifts. Cosmic ray and bad pixels are removed by comparison among the images during combination. Images are then recentered and the position of the center and all objects on the image are accurately tied to the J2000 coordinate system via the STScI Guide Star Catalog (Lasker et al. 1990). These images are flux-calibrated using the Oke-Gunn standard star observations, as detailed in our previous papers (Fan et al. 1996, Yan et al. 2000, Zhou et al. 2001, 2003).

We employ the method of Zheng et al. (1999) and Wu et al. (2002) (please see those papers for details of our methodology) to accurately determine the sky background in all three filters. Briefly, areas around M81 and M82 are first masked; M81 via a circle of 400 pixels in radius (22.7' in diameter) and M82 via a circle of 200 pixels in radius (11.4' in diameter). Stars are removed at $< 5\%$ of the sky level (cf. Zheng et al. 1998 and Wu et al. 2002) via PSF fitting and subtraction. The remaining areas around stars are then masked. The sky background is fit, using only the unmasked areas, using the same method as employed by Zheng et al. A smoothed version of the

masked image is produced by mode-filtering the image with a box 10×10 pixels in size. We then fit to each row of the smoothed-and-masked image a one-dimensional Legendre function of order 3 or less, rejecting points above 2σ on the high side and 3σ on the low side. The reason for the asymmetric rejection of points is that the main sources of scatter on the high side are faint, undetected sources and unfitted faint wings of stars, while the low side values result from statistical fluctuations.

The sky background that is fit is then subtracted from the h-, j- and t-images. The continuum component (stellar flux from M81) of the summed t-filter is obtained not from the image itself, but rather via interpolation of the stellar flux interpolated from the summed h- and j-images, suitably normalized by exposure times:

$$\text{Continuum}(t - \text{band}) = 0.45 \text{Continuum}(h - \text{band}) + 0.55 \text{Continuum}(j - \text{band}). \quad (1)$$

We then select ~ 50 un-saturated stars over the whole field of view, and adjust the interpolated values from the summed h- and j images such that these stars disappear. By doing this, we also properly scale the M81 stellar background in this interpolated image, assuming that none of these stars have emission lines in their spectra (and none did). The result of this sky background + stellar-M81-subtracted $\text{H}\alpha + [\text{NII}]$ image is shown in Fig. 3. It is evident from Figure 3 that all M81 starlight, as well as the flux from all foreground stars (not just the ones that are zeroed by our normalization process), are cleanly subtracted in the t-image via this interpolation procedure (modulo saturated stars).

To further demonstrate how well our subtraction procedure worked, Fig. 4 shows one-pixel-wide, 600-pixel-long slices through the t-image shown in Fig. 3. Fig. 4c,d,e,f are the slices through galaxy center. As can be seen, these slices go through several HII regions. (The center region is not shown in these slices, as steep luminosity gradients in the center of M81, combined with our lower angular resolution and slight mismatches in registration of images, result in large fluctuations in brightness on this scale from the continuum subtraction process.) It is evident from all six slices in Fig. 4 that our continuum-subtraction process has worked well in removing background flux in the $\text{H}\alpha$ part of the spectrum in our image (cf. the magnified view given in slices (a) and (b) of Fig. 4). Quantitatively the root-mean squared (RMS) statistical error in the background in the continuum-subtracted image is close to 15 ADU per pixel (close to $1.8 \times 10^{-16} \text{ergs s}^{-1} \text{cm}^{-2}$ per pixel), with an overall zero point residual of only 2 ADU per pixel ($2.4 \times 10^{-17} \text{ergs s}^{-1} \text{cm}^{-2}$ per pixel). The random background error of 15 ADU/pixel can be reduced by $1/\sqrt{n}$, where n is the number of the pixels sampled.

The small zero point error introduced resulting from our subtraction process does not enter significantly into the errors for the fluxes of the HII regions. This is because in the vicinity of every HII region there is always some diffuse emission which makes the boundaries of HII regions vague. Hence, we are specific about the area used around each HII region that was sampled to produce

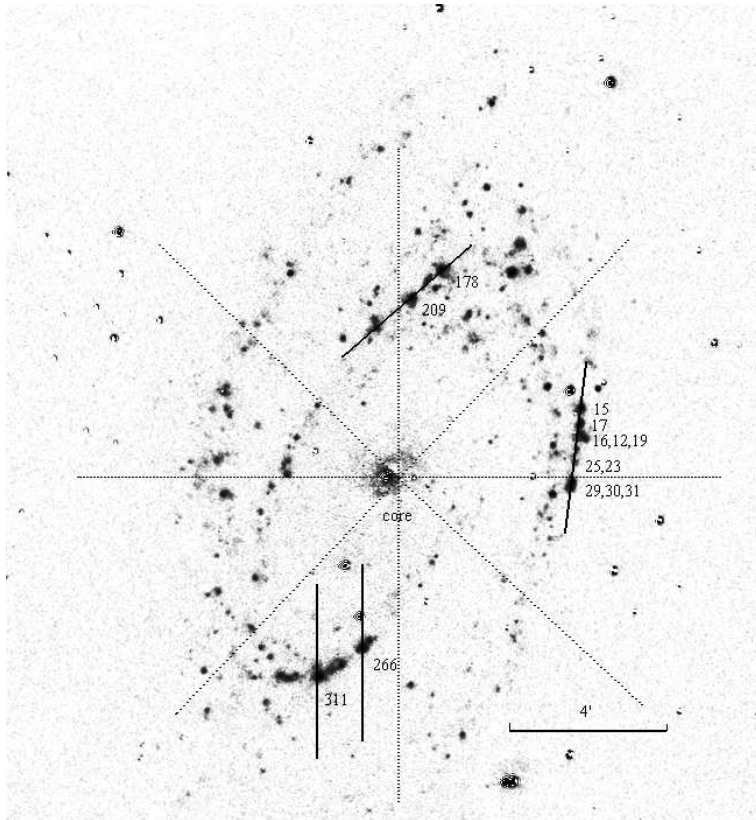


Fig. 3.— The sky background-subtracted H α image. The positions of long-slit spectroscopic observations are overlaid as solid lines. Slices taken through this image to test for accuracy of background subtraction are given as dotted lines. The PKS numbers of the HII regions are also given. Note that up is north and left is east.

its reported flux. The error and S/N for the $H\alpha + [NII]$ fluxes from the HII regions in this paper include just the calibration error and the random background error for each region; Zero point errors in the continuum-subtracted image are thus included in the background subtraction for each HII region. As stated above, we only use those HII regions with S/N values for their fluxes that are $3\text{-}\sigma$ or higher.

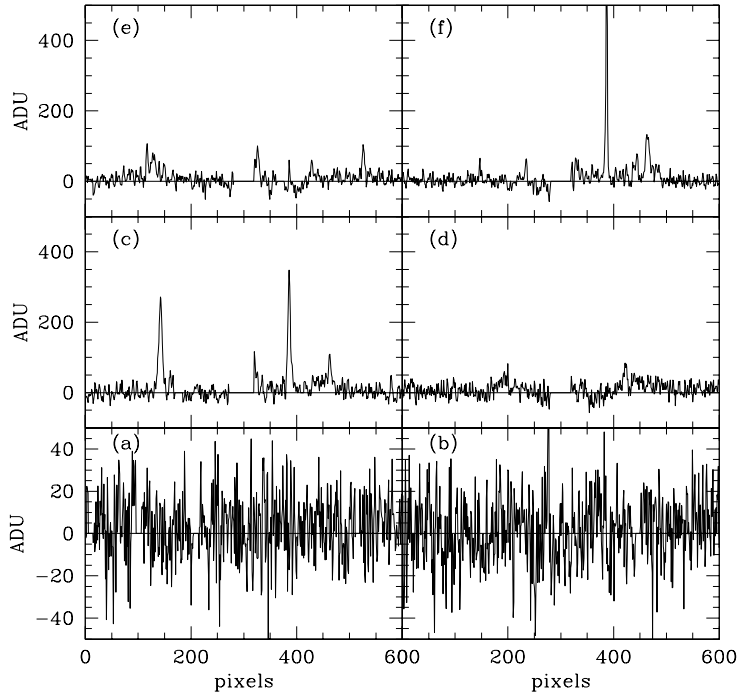


Fig. 4.— Six slices through Fig. 3 that are each one pixel wide and 600 pixels long, shown as dotted lines in Fig. 3. Slices (a) and (b) are cuts along the Y direction through the left-hand and right sides regions in Fig. 3 where there are no HII regions. Slices (c), (d), (e) and (f) each go through the center of M81 and a few HII regions, with the galaxy center located at pixel 300 in each slice. Slices (c) and (d) are cuts along the X and Y directions, respectively. Slice (e) is along a diagonal that goes from left-bottom to right-top, while slice (f) is a diagonal that goes from left-top to right-bottom. In slices (c)–(f) then galaxy center $H\alpha$ goes off scale.

2.4. Flux measurements and calibration of the $H\alpha$ emission

The $H\alpha + [NII]$ emission from the M81 HII regions are calibrated by the $H\alpha + [NII]$ emission we measure for the 10 HII regions with reasonably high S/N spectra in the 2.1m data. To do so, we employ the intermediate-band fluxes in our images that we obtain for M81 outside the HII regions via our standard star calibrations. In Table 3 we give the combined $H\alpha + [NII]$ emission flux in

the continuum-flux-calibrated spectra together with the ADU counts for $H\alpha + [NII]$ emission as measured from our image.

Table 3: Calibrated $H\alpha$ emission fluxes for Spectroscopically-Observed HII regions

PKS-index	Flux(t-filter)*	Flux(line)	EW(\AA)	ADU($H\alpha$)
15	1.93e-14	2.00e-13	1066.0	17350.8
16	3.08e-14	1.04e-13	363.4	6337.0
17	2.32e-14	1.97e-13	849.4	13566.0
23	1.48e-14	4.87e-14	321.2	3531.5
25	1.88e-14	3.06e-14	146.0	2492.9
29	3.89e-14	2.92e-13	739.7	23072.5
178	8.85e-14	2.34e-13	261.6	22110.4
209	7.75e-14	1.54e-13	185.6	7668.3
266	7.99e-14	1.36e-13	149.5	14884.5
311	8.79e-14	3.81e-13	412.7	29521.9

*Flux(t-filter) means the flux integrated over the t-filter passband.

Fig. 5 shows the relationship we derive between the $H\alpha + [NII]$ fluxes from the HII regions obtained from the spectra and the ADU counts we measure for these same HII regions from the continuum-subtracted t-image. It is evident that there is a good relationship between spectrally-derived fluxes and ADU values on the image, yielding a relation of

$$\text{Flux}(H\alpha + N[II]) = 1.34 \pm 0.10 \times 10^{-4} \text{ADU}(H\alpha + N[II]), \quad (2)$$

where $\text{ADU}(H\alpha + N[II])$ is the pixel values for the continuum-subtracted t-band image, and $\text{Flux}(H\alpha + N[II])$ is the integral flux over the $H\alpha$ filter pass band in units of $10^{-13} \text{ergs s}^{-1} \text{cm}^{-2}$.

Using this calibration, $H\alpha + [NII]$ fluxes are obtained for all the HII regions in M81 from the continuum-subtracted $H\alpha + [NII]$ image, using circular apertures that, on average, are $2.5''$ larger in radius than those of PKS. Because of the low space resolution of our images, when we made independent flux measurements of HII regions using the ‘‘SExtractor’’ code (Bertin 1996), the number of regions found was less than that of PKS. This depends on what threshold of flux and other parameters for the detection. Thus for simplicity, we adopt the positions of HII regions provided by PKS.

2.5. The HII Region Catalog

The resulting coordinates and fluxes of the HII regions are listed in Table 4. The galaxy center of M81 is located at $\alpha = 09\text{h}55\text{m}33.2\text{s}$, $\delta = +69^\circ 03' 55''$ (J2000.0), In this table: column 1 is the

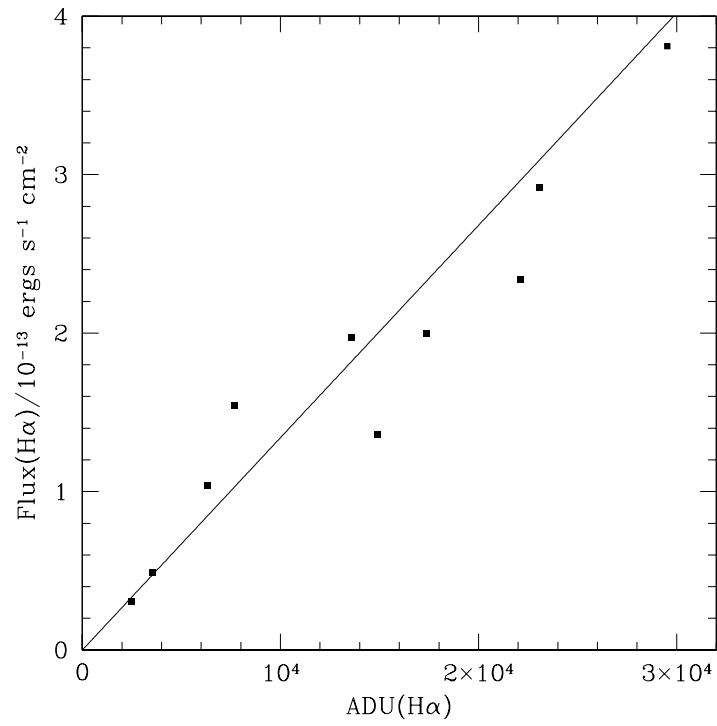


Fig. 5.— The ADU vs flux relation for the calibration HII regions listed in Table 3. Flux is given in units of 10^{-13} ergs s⁻¹ cm⁻². The solid line represents the relation given by Eq.(3).

PKS number for the HII region; columns 2 and 3 give the RA, DEC coordinates (J2000) of the HII regions; columns 4 and 5 list X, Y distance from the galaxy center, in unit of arc-second; columns 6, 7 and 9 list the $H\alpha + [NII]$ flux measured in this paper for this HII region, its 1σ uncertainty, and the PKS-flux (Flux^{*}) respectively, in units of $10^{-16}\text{ergs s}^{-1}\text{cm}^{-2}$; column 8 is the diameter of the circular aperture used to measure the flux for each HII region, in units of arc-seconds; column 10 is the signal-to-noise (S/N) value for each HII region from our measurement. Kindly note that the direction of X (or Y) axis is the same as RA (or DEC). The full table is in electronic form; only the first 15 lines are printed here.

Please note that our X, Y values are slightly different than those of PKS because our astrometry puts the center of M81 in a different location, with an additional rotation of the field of view. Of the 492 HII regions for which we have obtained $H\alpha + [NII]$ fluxes, 93% (456) have those fluxes determined to an accuracy of $3\text{-}\sigma$ or greater. We will only use these more accurately-determined fluxes in our analysis.

3. Estimation of Errors and Discussion

Our errors come from a combination of errors in HII region pointing during the spectral observations, differences of matching the area of the HII regions on the image to that covered by the spectra, the seeing difference between the image and the spectra, flux calibration of the image observations, and how well we can continuum-subtract the background from the HII regions on the $H\alpha$ image.

3.1. Pointing Errors

For the 10 bright HII regions for which we obtained spectra, we define on the $H\alpha$ image the same rectangle area in the same direction as the spectrograph slit. Fortunately, the seeing of the spectroscopic observations is similar to that of the CCD image, 4 ± 0.2 arc-second. Our internal estimate of the error of telescope pointing (obtained from the PIPELINE 1 fit to the Lasker et al. stars) is 0.3 arc-second. Assuming the PSF is Gaussian with a FWHM of 4 arc-seconds, we calculate the ratio of flux for various stars for offsets in position up to 0.5 pixel ($0.85''$) for the spectroscopic slit width. We find that the difference is 0.02 mag when the offset is 0.5 pixel. We therefore conclude that the uncertainty from telescope pointing introduced into our data is less than 0.02 mag.

3.2. Absolute Calibration and Linearity

As shown in Fig. 3 and §2.4, we match the $H\alpha + [NII]$ fluxes from our spectral observations to the ADU counts on the continuum-subtracted image to an accuracy of 7%. Any error caused by mismatch of slit area with image area for these HII regions is subsumed into this calibration. As discussed in previous papers from our program (Fan et al. 1996, Yan et al. 2000, Zhou et al. 2001, 2003), the uncertainty in calibrating the intermediate-band images is generally less than 0.02 mag, or 2% in flux. To be more conservative, we allow an error of 3% in flux. Taken together in quadrature, this yields a total zero point absolute spectrophotometry calibration error of close to 8%.

We demonstrate the overall linearity of the $H\alpha$ image by differentially comparing the fluxes determined for the HII regions from the $H\alpha + [NII]$ t-image from those determined for those same regions from the wider, intermediate-band i-image which covers this spectral region. This is shown in Fig. 6, where we plot the difference, $H\alpha + [NII]$ flux from the t-image minus that obtained from the i-band image versus t-image $H\alpha + [NII]$ flux for the brighter HII regions, including the 10 brightest HII regions that were used for the spectral-line calibration.

In this comparison the i-band magnitudes are set so that the i-band magnitudes for bright HII regions are equal to the corresponding t-band magnitudes, as what is relevant in this comparison is the linearity of the the $H\alpha$ scale. Further, for this comparison we do not subtract the background of M81 for the i-band HII regions. We also note that the BATC i filter also includes emission from [SII] doublet at 6717\AA and 6737\AA , further complicating this comparison. As such, we limit our comparison to the brighter HII regions. As can be seen in Fig. 6, these two independent magnitude measures of the HII regions of M81 are reasonably linear.

3.3. Comparison with previous work

The HII region fluxes measured by PKS were made from photographic plates. As such, we might expect some systematic differences between their fluxes and ours as a function of position on M81, given the well-known difficulty of flat-fielding photographic images. In Fig. 7a we show the ratio of fluxes, this paper to that of PKS, as function of our fluxes. Given that our apertures are larger than those of PKS, we naturally expect our fluxes to be higher, which is what we find. We also find there to be a systematic effect over the field of view. Fig. 7b shows the ratio used in Fig. 7a plotted versus radial position from the center of the galaxy.

As is evident, there is a systematic difference in fluxes as a function of increasing distance going from the south-east to the north-west part of M81. On this same graph, we plot (with solid symbols) the difference between our $H\alpha$ fluxes and our i-band fluxes (t-flux/i-flux) along the same diagonal. As there is no evidence that such a systematic error exists in our data, we conclude that the photographic data of PKS contains this error.

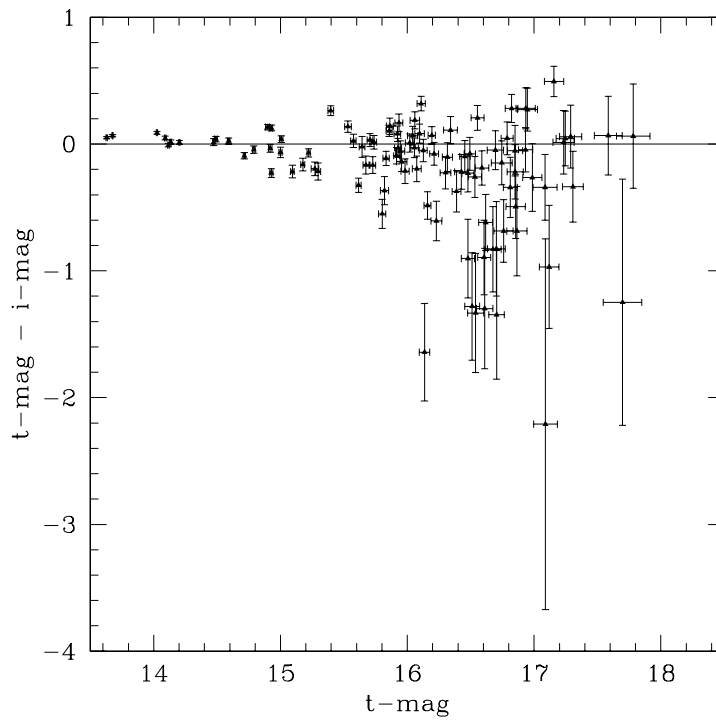


Fig. 6.— The plot of $t\text{-mag}$ (the $H\alpha$ instrumental magnitudes measured from continuum-subtracted t -filter image) vs. the difference between $t\text{-mag}$ and $i\text{-mag}$ (the instrumental magnitudes measured from the continuum-subtracted i -filter image). See main text for details.

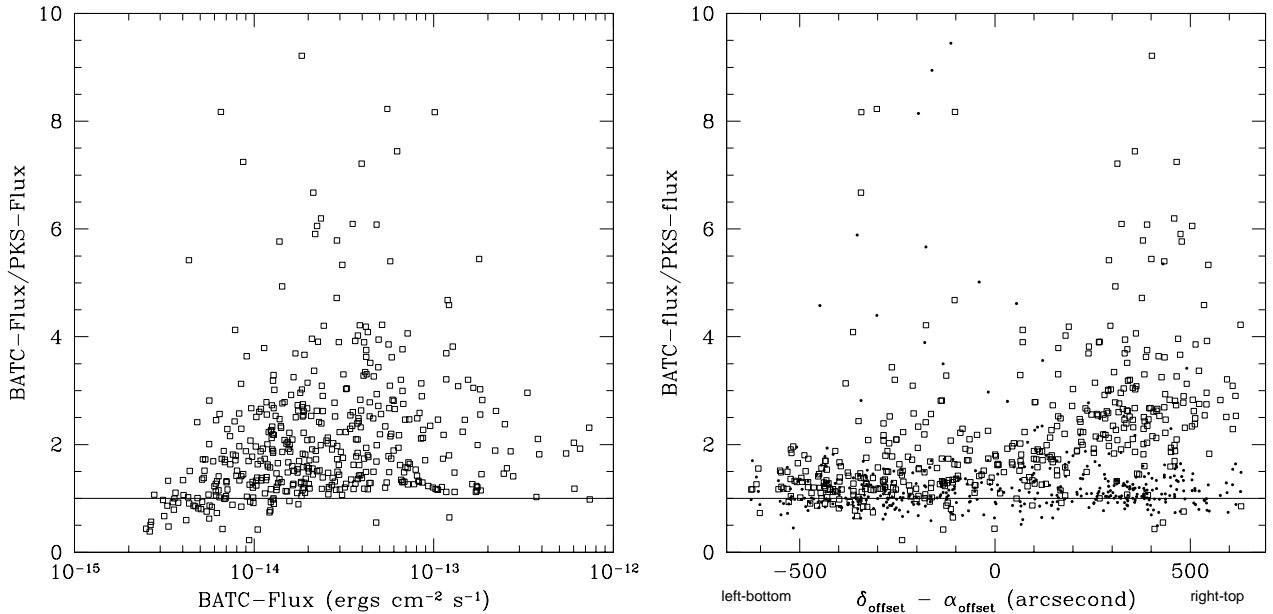


Fig. 7.— Left panel: the plot of ratio of flux to PKS-flux vs. BATC-flux. Right panel: The plot of ratio of BATC-flux to PKS-flux vs. $(\delta_{offset} - \alpha_{offset})$ going in a diagonal from the south-west (left-bottom) to the north-east (right-top) as indicated by the dashed line in Fig. 3.

3.4. Total H α Flux From Observed M81 HII Regions and SN 1993J

The total H α + [NII] flux of all the HII regions (with S/N $\geq 3\sigma$) in M81 is $\sim 2.26 \times 10^{-11} \text{ ergs s}^{-1} \text{ cm}^{-2}$ which corresponds to a luminosity of $\sim 8.7 \times 10^6 L_{\odot}$ (the fainter, lower S/N HII regions in M81 contribute less than 1% additional flux). The total H α + [NII] flux we measure is half of the overall H α + [NII] emission coming from M81, $(1.77 \pm 0.53) \times 10^7 L_{\odot}$ (Devereux et al. 1995; including both HII region and diffuse emission-line flux). Similarly, the study of Greenawalt et al. (1998) attributes about half of the H α emission to the DIG, so the effect of adding in the [NII] emission to the H α emission seems not to affect this ratio. In addition, Devereux et al.(1995) find that about 17% of the flux is due to emission by the nuclear spiral, leaving 1/3 of the H α + [NII] flux from M81 coming from its diffuse interstellar medium,

We also note that we detect extra H α + [NII] emission located at an inner arm of M81 at pixel position of (926.4, 428.6), corresponding to $\alpha = 09^{\text{h}}55^{\text{m}}24^{\text{s}}.7, \delta = +69^{\circ}01'15''$ (J2000.0). The position is consistent with that of the X-ray source studied by Immler & Wang (2001). Therefore we identify this emission spot as coming from the remnant of the Type IIb supernova SN 1993J (cf. Fig 2.). The flux is $5.8 \times 10^{-14} \text{ ergs s}^{-1} \text{ cm}^{-2}$, measured over the time period 11 Feb 1995 to 19 Feb 1995.

3.5. The Luminosity Function of H81 HII Regions

The $H\alpha + [\text{NII}]$ luminosity functions of the HII regions in M81 have been determined before (cf. PKS and references therein; Kennicutt et al. 1989), primarily in the form of a power law. As Scoville, et al. (2001) point out, angular resolution issues cause ground-based data to blend HII regions together, relative to better-resolved images. This is especially true for the BATC data, which has a relative poor angular resolution ($\text{FWHM} = 4''$). Following Scoville, et al. we define the differential form of the luminosity function as

$$\frac{dN(F_{H\alpha})}{d \ln F_{H\alpha}} = N_{up} (F_{H\alpha}/F_{up})^\alpha \quad (3)$$

where F_{up} is the $H\alpha$ for the brightest HII region and $F_{H\alpha}$ are the fluxes measured, N_{up} is approximately the number of regions between $0.5 F_{up}$ and F_{up} for $\alpha \sim 1$. We selected only those HII regions with $S/N \geq 3$ (456 regions in total) and apply the linear fitting using equation above. The slope α was found to be -0.70 (little different than what is obtained from 492 regions, $\alpha = -0.71$). This result is in agreement with previous results by PKS and Kennicutt et al. (1989).

3.6. Lyman continuum emission rate and star formation rate

The observed $H\alpha + [\text{NII}]$ luminosities of the HII regions in M81 with $S/N \geq 3\sigma$ range from $3.9 \times 10^{36} \text{ergs s}^{-1}$ to $1.2 \times 10^{39} \text{ergs s}^{-1}$. Applying an average extinction of $A_V = 1.1 \pm 0.4 \text{ mag}$ (cf. Kaufman, Bash & Hodge 1987) for the HII regions, we find a correction factor to the $H\alpha + [\text{NII}]$ luminosities should be $10^{0.320 \times A_V} \simeq 2.2$ (Rieke & Lebofsky 1985). Assuming Brocklehurst (1970) Case B recombination and neglecting absorption by He, the required Lyman continuum emission rate, Q_{LyC} is estimated to be

$$Q_{LyC} = 7.32 \times 10^{11} L_{H\alpha} \left(\frac{T_e}{10^4 K} \right)^{0.11} \text{ s}^{-1}$$

(Osterbrock 1989). For $T_e = 10^4 K$, we find Q_{LyC} ranges from $2.6 \times 10^{48} \text{ s}^{-1}$ to $1.9 \times 10^{51} \text{ s}^{-1}$.

Stellar synthesis models suggest that the star formation rate (SFR) is related to $L_{H\alpha}$ by

$$\text{SFR} = \frac{L_{H\alpha}(\text{total})}{1.12 \times 10^{41} \text{ergs s}^{-1}} M_\odot \text{yr}^{-1}$$

(Kennicutt 1983). Using this conversion factor, and taking the $H\alpha + [\text{NII}]$ luminosity of M81 to be $3.5 \times 10^{40} \text{ergs s}^{-1}$, we obtain a SFR of $\sim 0.31 M_\odot \text{yr}^{-1}$. With extinction correction, this value becomes $\sim 0.68 M_\odot \text{yr}^{-1}$, or 3.6 times higher than the value of 0.19 solar mass per year obtained by Hill et al. 1995 from space-based UV observations (applying to their data the same extinction value as we use).

4. Summary

As part of the ongoing BATC survey, $H\alpha + [\text{NII}]$ emission measurements of the HII regions of M81 in this paper are made to test our methodology of calibrating these fluxes. Our methods take advantage of both spectra and the well-calibrated intermediate-band images we have obtained of this galaxy in neighboring passbands. We also employ our previously well-tested background subtraction techniques (developed over the past few years by our team) to reduce uncertainties associated with continuum subtraction of the narrow band image centered on $H\alpha + [\text{NII}]$. We find the zero point uncertainty of $H\alpha + [\text{NII}]$ flux is close to 8% for bright HII regions. A comparison of our results with those Petit, Sivan & Karachentsev (1988) uncovers a systematic error in their fluxes as a function of position on their photographic plates. As a result, a new, more accurate catalog of the $H\alpha + [\text{NII}]$ emission from the HII regions in M81 is given. The total $H\alpha + [\text{NII}]$ emission luminosity for 456 HII regions is $\sim 8.7 \times 10^6 L_{\odot}$. The differential power-law function of number of the HII regions per logarithmic flux interval is investigated and the slope of that power law found to be -0.70 , consistent with previous work. The derived star formation rate for all of the HII regions is $\sim 0.68 M_{\odot} \text{ yr}^{-1}$, 3.6 times higher than that previously obtained from UV-based studies (Hill et al. 1995).

WPL acknowledges supports from NKBRFSF G1999075402 and the Shanghai NSF grant 02ZA4093. WPL thanks the exchange program between Chinese Academic of Sciences and Max-Planck Society and the hospitality from Max-Planck-Institute for Astrophysics. The authors also thank the anonymous referee for helpful comments. This work is supported partly by the NSFC grant 19833020, 10203004 and by the US NFS grant INT-9301805.

REFERENCES

- Adler D.S., & Westpfahl D.J., 1996, *AJ*, 111, 735
- Brocklehurst M., 1970, *MNRAS*, 148, 417
- Davidge T.J., & Courteau S., 1999, *AJ*, 117, 2781
- Devereux, N.A., Jacoby G., Ciardullo R., 1995, *AJ*, 110, 1115
- Fan X., et al., 1996, *AJ*, 112, 628
- Freedman W.L., et al., 1994, *ApJ*, 427, 628
- Garnett D.R., & Shields G.A., 1987, *ApJ*, 317, 82
- Greenawalt B., Walterbos R.A.M., Thilker D., & Hoopes C.G., 1998, *ApJ*, 506, 135
- Grossan B., et al. 2001, *ApJ*, 563, 687

Table 4: The catalog of optical bright HII regions with H α flux

No	α	δ	X	Y	Flux	Err	D	Flux*	S/N
1	09h54m19.82s	69°07'53.1''	-392.1	238.1	47.	7.	6.6	55.	6.9
2	09h54m23.99s	69°08'02.2''	-369.8	247.2	132.	8.	6.6	52.	17.3
3	09h54m33.49s	69°09'04.8''	-318.8	309.8	1.	5.	5.5	28.	0.3
4	09h54m34.67s	69°05'52.2''	-313.2	117.2	477.	10.	6.6	866.	45.8
5	09h54m36.10s	69°06'30.5''	-305.4	155.5	599.	14.	12.0	213.	42.9
6	09h54m35.74s	69°09'04.3''	-306.8	309.3	241.	10.	8.8	83.	23.3
7	09h54m36.08s	69°07'16.2''	-305.4	201.2	391.	12.	9.7	138.	32.9
8	09h54m36.60s	69°06'32.3''	-302.7	157.3	482.	11.	9.7	242.	43.9
9	09h54m36.27s	69°07'15.4''	-304.3	200.4	538.	14.	12.0	230.	37.3
10	09h54m37.17s	69°04'57.8''	-300.1	62.8	129.	44.	6.6	42.	3.0
11	09h54m37.35s	69°06'35.5''	-298.7	160.5	235.	9.	6.6	38.	26.8
12	09h54m38.53s	69°04'42.2''	-292.8	47.2	1754.	56.	10.5	881.	31.2
13	09h54m38.73s	69°06'49.1''	-291.3	174.1	163.	12.	7.9	78.	13.7
14	09h54m39.15s	69°05'35.1''	-289.3	100.1	480.	50.	7.9	79.	9.6
1993J	09h55m24.72s	69°01'15.0''	-45.5	-160.0	582.	19.	13.6	-	30.6

Hill J.K., et al. 1992, ApJ, 395, 37

Hill J.K., et al. 1995, ApJ, 438, 181

Hodge P.W., & Kennicutt R.C., 1983a, ApJ, 88, 296

Hodge P.W., & Kennicutt R.C., 1983b, ApJ, 267, 563

Immler S., & Wang Q.D., ApJ, 554, 202

Kaufman M., Kennicutt R. C., Bash F. N., 1986, IAU Circ., 116, 503

Kaufman M., Bash F.N., Kennicutt R.C., & Hodge P.W., 1987, ApJ, 319, 61

Keel W.C., 1989, AJ, 98, 195

Kennicutt R.C., Jr., Edgar, B.K., Hodge, P.W., 1989, ApJ, 337, 761

Kennicutt R.C., 1983, ApJ, 272, 54

Kong X., Lin W.P., Zhou X., Chen F.Z., & Chen J.S., 1999, Progress in Natural Sciences (China), 9, 1083

Kong X., et al., 2000, AJ, 119, 2745

Lasker B.M., et al., 1990, AJ, 99, 2019

- Matheson T., et al., 2000, AJ, 120, 1499
- Oke J.B., & Gunn J.E., 1983, ApJ, 266, 713
- Osterbrock D.E., 1989, Astrophysics of gaseous nebulae and active galactic nuclei (Mill Valley, California: University Sciences Books)
- Petit H., Sivan J. -P., Karachentsev I. D., 1988, A&AS, 74, 475 (PKS)
- Rieke G.H., & Lebofsky M.J., 1985, 288, 618
- Scoville N.Z., et al., 2001, AJ, 122, 3017
- Stauffer, J.R., & Bothun, G.D., 1984, AJ, 89, 1702
- Wu H., et al., 2002, AJ, 123, 1364
- Yan H.J., et al., 2000, PASP, 112, 691
- Zheng Z.Y., et al. 1999, AJ, 117, 2757
- Zhou X., et al. 2001, ChJAA, Vol.1, No.4, 372
- Zhou X., et al., 2003, A&A, 397, 361